Journal of Power Sources 188 (2009) 538–545

Contents lists available at ScienceDirect

Journal of Power Sources

journal homepage: www.elsevier.com/locate/jpowsour

A modified ZrO_2-coating process to improve electrochemical performance of $Li(Ni_{1/3}Co_{1/3}Mn_{1/3})O_2$

Youyuan Huang, Jitao Chen, Jiangfeng Ni, Henghui Zhou*, Xinxiang Zhang

College of Chemistry and Molecular Engineering, Peking University, Beijing 100871, PR China

ARTICLE INFO

Article history:
Received 30 July 2008
Received in revised form 10 December 2008
Accepted 11 December 2008
Available online 24 December 2008

Keywords:
Lithium ion batteries
$Li(Ni_{1/3}Co_{1/3}Mn_{1/3})O_2$
ZrO_2 coating
Modification

ABSTRACT

A modified Zr-coating process was introduced to improve the electrochemical performance of $Li(Ni_{1/3}Co_{1/3}Mn_{1/3})O_2$. The ZrO_2-coating was carried out on an intermediate, $(Ni_{1/3}Co_{1/3}Mn_{1/3})(OH)_2$, rather than on $Li(Ni_{1/3}Co_{1/3}Mn_{1/3})O_2$. After a heat treatment process, one part of the Zr covered the surface of $Li(Ni_{1/3}Co_{1/3}Mn_{1/3})O_2$ in the form of a Li_2ZrO_3 coating layer, and the other part diffused into the crystal lattice of $Li(Ni_{1/3}Co_{1/3}Mn_{1/3})O_2$. A decreasing gradient distribution in the concentration of Zr was detected from the surface to the bulk of $Li(Ni_{1/3}Co_{1/3}Mn_{1/3})O_2$ by X-ray photoelectron spectra (XPS). Electrochemical tests indicated that the 1% (Zr/Ni + Co + Mn) ZrO_2-modified $Li(Ni_{1/3}Co_{1/3}Mn_{1/3})O_2$ prepared by this process showed better cyclability and rate capability than bare $Li(Ni_{1/3}Co_{1/3}Mn_{1/3})O_2$. The result can be ascribed to the special effect of Zr in ZrO_2-modified $Li(Ni_{1/3}Co_{1/3}Mn_{1/3})O_2$. The surface coating layer of Li_2ZrO_3 improved the cycle performance, while the incorporation of Zr in the crystal lattice of $Li(Ni_{1/3}Co_{1/3}Mn_{1/3})O_2$ modified the rate capability by increasing the lattice parameters. Electrochemical impedance spectra (EIS) results showed that the increase of charge transfer resistance during cycling was suppressed significantly by ZrO_2 modification.

1. Introduction

Recently, layered $Li(Ni_{1/3}Co_{1/3}Mn_{1/3})O_2$ has been considered a promising alternative to conventional $LiCoO_2$ cathodes for lithium ion batteries due to its reduced cost, enhanced safety and increased energy density [1–4]. However, there are still two important problems limiting its application in high power lithium ion batteries for EV and HEV. One is the severe capacity fading when it is charged to 4.5 V or higher [5–7]; the other is its relatively poor rate capability due to its lower electronic conductivity compared to $LiCoO_2$ [8–10]. It has been proven that coating with inert metal oxides, such as ZnO [11], MgO [12], Al_2O_3 [13,14], ZrO_2 [15–18], TiO_2 [19,20], can significantly improve the cycle performance of layered cathode materials. Specifically, Al_2O_3, TiO_2, and ZrO_2 coatings have been employed to enhance the cycle performance of $Li(Ni_{1/3}Co_{1/3}Mn_{1/3})O_2$ at a high cut-off voltage [21,22]. The inert coating layer can improve the interphase stability between the electrode and electrolyte. Nevertheless, these inert oxides are usually poor electronic and ionic conductors. A coating layer of inert oxides often leads to a reduced reversible capacity and a poorer rate discharging ability. Compared to these metal oxides, some Li-contain oxides, such as $LiAlO_2$ [23,24], are more effective for enhancing the electrochemical performance of $Li(Ni_{1/3}Co_{1/3}Mn_{1/3})O_2$ because they have high Li^+ conductivity and can provide the tunnel for Li^+ transportation during charging and discharging processes.

In this paper, a new process is introduced to enhance the rate capability and cycle performance of $Li(Ni_{1/3}Co_{1/3}Mn_{1/3})O_2$. In this process, ZrO_2 was coated on $(Ni_{1/3}Co_{1/3}Mn_{1/3})(OH)_2$ instead of $Li(Ni_{1/3}Co_{1/3}Mn_{1/3})O_2$. ZrO_2-modified $Li(Ni_{1/3}Co_{1/3}Mn_{1/3})O_2$ was synthesized by sintering the mixture of ZrO_2-coated $(Ni_{1/3}Co_{1/3}Mn_{1/3})(OH)_2$ and Li_2CO_3. After the high temperature treatment, one part of the Zr existed on the surface of the $Li(Ni_{1/3}Co_{1/3}Mn_{1/3})O_2$ as a Li_2ZrO_3 coating layer, and the other part of Zr was diffused into the $Li(Ni_{1/3}Co_{1/3}Mn_{1/3})O_2$ bulk and modified its crystal structure. To our knowledge, this is the first attempt by such means to improve the electrochemical properties of layered cathode materials. The structure, surface character, and electrochemical performance of ZrO_2-modified $Li(Ni_{1/3}Co_{1/3}Mn_{1/3})O_2$ synthesized by this process have been thoroughly investigated.

2. Experimental

2.1. Synthesis of ZrO_2-modified $Li(Ni_{1/3}Co_{1/3}Mn_{1/3})O_2$

$(Ni_{1/3}Co_{1/3}Mn_{1/3})(OH)_2$ was prepared by co-precipitation from a solution containing stoichiometric amounts of nickel/cobalt/manganese nitrates by the addition of NaOH and NH_3–H_2O solution. $(Ni_{1/3}Co_{1/3}Mn_{1/3})(OH)_2$ with 8–10 μm diam-

* Corresponding author. Tel.: +86 10 62757908; fax: +86 10 62757908.
E-mail address: hhzhou@pku.edu.cn (H. Zhou).

0378-7753/$ – see front matter © 2008 Elsevier B.V. All rights reserved.
doi:10.1016/j.jpowsour.2008.12.037

eter was prepared by controlling the reaction condition. To coat $(Ni_{1/3}Co_{1/3}Mn_{1/3})(OH)_2$ with ZrO_2, $ZrO(NO_3)_2$ was first dissolved in ethanol at room temperature. The $(Ni_{1/3}Co_{1/3}Mn_{1/3})(OH)_2$ powder was poured into the solution with continuous stirring for 1 h, and then NH_3–H_2O (2%) was slowly added into the solution and thoroughly mixed for 30 min. This mixture was kept at 80 °C for 5 h until most of the solvent was evaporated. The powder was dried at 120 °C for 12 h to obtain the precursor of ZrO_2-coated $(Ni_{1/3}Co_{1/3}Mn_{1/3})(OH)_2$. The Zr content was set at molar ratios of Zr/(Ni + Co + Mn) = 0.5, 1, 2, 3% by controlling the amount of $ZrO(NO_3)_2$. To prepare ZrO_2-modified $Li(Ni_{1/3}Co_{1/3}Mn_{1/3})O_2$ powder, the as-prepared ZrO_2-coated $(Ni_{1/3}Co_{1/3}Mn_{1/3})(OH)_2$ and Li_2CO_3 were mixed and calcined at 900 °C for 24 h. Li_2CO_3 amount was set at molar ratios of Li/(Ni + Co + Mn + Zr) = 1.03.

2.2. Characterization of the structure and physical parameters

X-ray diffractometry (XRD, Rigaku Rint 2200) was employed to characterize the crystal structure of the powder. XRD data were obtained with Cu Kα radiation (λ = 0.15406 nm) in the 2θ range of 10–80° at a continuous scan mode with a step size of 0.02° and a scan rate of 2° min^{-1}. The particle shape and morphology images of $Li(Ni_{1/3}Co_{1/3}Mn_{1/3})O_2$ were observed with a scanning electron microscope (SEM, Hitachi S-3500N). Energy dispersive X-ray spectroscopy (EDS, Oxford INCA) was employed to analyze the composition and spatial distribution of transition metal elements on the surfaces of materials. The tap density of materials was measured using a tap density tester (FTZ-4, 300 times/min for 3000 taps). ICP-AES (IRIS Intrepid II, USA) was employed to measure the transition metal element content of materials. X-ray photoelectron spectroscopy (XPS, Kratos Axis Ultra spectrometer with Al Kα radiation, $h\nu$ = 1486.71 eV) measurements were performed to investigate information on the surface of ZrO_2-modified $Li(Ni_{1/3}Co_{1/3}Mn_{1/3})O_2$. Macro-mode (about 4 mm × 4 mm) Ar-ion etching was employed to assist XPS in measuring the concentrations of transition metal elements at different depths from the surface into the bulk of the ZrO_2-modified $Li(Ni_{1/3}Co_{1/3}Mn_{1/3})O_2$. The etching rate was estimated as 0.5 nm min^{-1} for a silica patch.

2.3. Electrochemical measurements

The electrode was fabricated from a 93:4:3 (mass%) mixture of active material:Super-P carbon black:polyvinylidene difluoride (PVDF). The PVDF was dissolved in N-methylpyrrolidinone (NMP), and then the active material and Super-P carbon black were added. After homogenization, the slurry was evacuated for 20 min to remove any residual air. The slurry was coated on a thin aluminum foil (20 μm thick) and dried overnight at 120 °C in a vacuum oven. The electrode was pressed at a pressure of 15–20 MPa and punched into round disks 10 mm in diameter. The thickness of the cathode film was about 50 μm. Standard 2032 coin cells were assembled in a dry room to test the electrochemical properties of the cathode material. Lithium metal foil was used as the counter electrode and 1.0 mol L^{-1} $LiPF_6$/(EC:EMC:DEC = 1:1:1) as the electrolyte. After aging for 10 h to ensure full wetting of the electrolyte, the cell was charged and discharged for three cycles at a current density of 0.2*C* (150 mA g^{-1} was assumed to be the 1*C* rate) in the range of 4.3–3.0 V (vs. Li^+/Li) for activation. The rate capability was measured by charging the cells to 4.3 V at a low current density and then discharging at current densities of 0.2*C*, 0.5*C*, 1.0*C*, 2.0*C*, 3.0*C*, and 5.0*C*. The electrochemical impedance spectroscopy (EIS) of the coin cell was measured in the frequency range from 1 mHz to 100 kHz at a CHI660B electrochemistry work station.

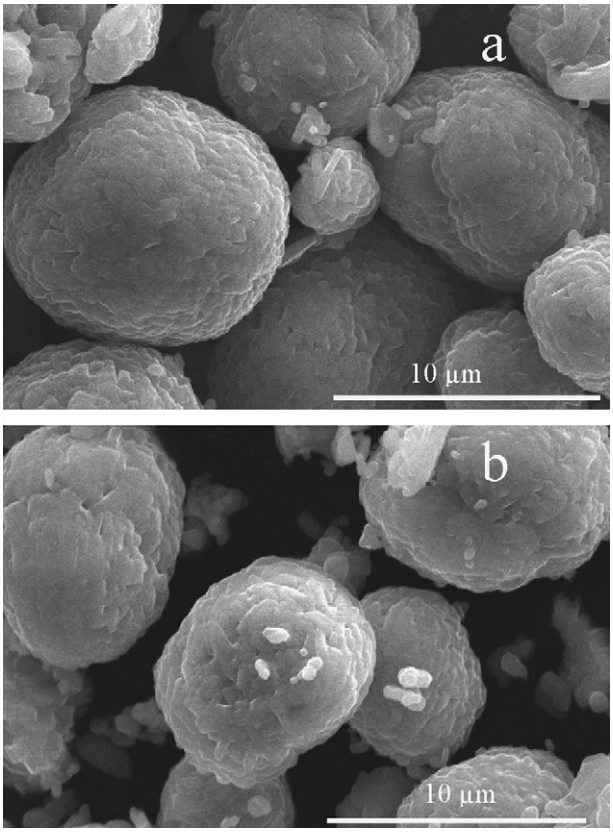

Fig. 1. SEM images of bare (a) and 1% ZrO_2-modified $Li(Ni_{1/3}Co_{1/3}Mn_{1/3})O_2$ (b).

3. Results and discussion

3.1. Morphology of ZrO_2-modified $Li(Ni_{1/3}Co_{1/3}Mn_{1/3})O_2$

SEM images of bare and 1% ZrO_2-modified $Li(Ni_{1/3}Co_{1/3}Mn_{1/3})O_2$ are given in Fig. 1. All samples have good spheral shape with diameters of about 8 μm. The spheral particle is beneficial for achieving a high tap density and energy density. The test results show that the tap densities of these samples reach 2.4 g cm^{-3}. No significant difference between the bare and 1% ZrO_2-modified $Li(Ni_{1/3}Co_{1/3}Mn_{1/3})O_2$ was detected by SEM. The composition and distribution of elements on the surface of 1% ZrO_2-modified $Li(Ni_{1/3}Co_{1/3}Mn_{1/3})O_2$ were examined by EDS, as shown in Fig. 2. According to Fig. 2, Zr is distributed uniformly on the surface of particles of 1% ZrO_2-modified $Li(Ni_{1/3}Co_{1/3}Mn_{1/3})O_2$. A further discussion on the surface configuration and the distribution of Zr along the radial direction of particles will be done in the next section. To confirm the ratio of Ni:Co:Mn, Ni, Co, Mn concentratoins in $(Ni_{1/3}Co_{1/3}Mn_{1/3})(OH)_2$ and 1% ZrO_2-modified $Li(Ni_{1/3}Co_{1/3}Mn_{1/3})O_2$ were measured by ICP-AES, and the results are given in Table 1. The results show that the ratio of Ni:Co:Mn is close to 1:1:1. Zr concentrations of different amounts in ZrO_2-modified samples were also measured by ICP-AES. The results indicate that the ratio of Zr/(Ni + Co + Mn) (not shown) is in good agreement with the initial ratio in the mixture.

3.2. Analysis of the crystal structures of ZrO_2-modified $Li(Ni_{1/3}Co_{1/3}Mn_{1/3})O_2$

The crystal structures of the bare and ZrO_2-modified $Li(Ni_{1/3}Co_{1/3}Mn_{1/3})O_2$ materials with different amounts of Zr were investigated by XRD, as shown in Fig. 3. Diffraction patterns of all samples can be identified as a layered α-$NaFeO_2$

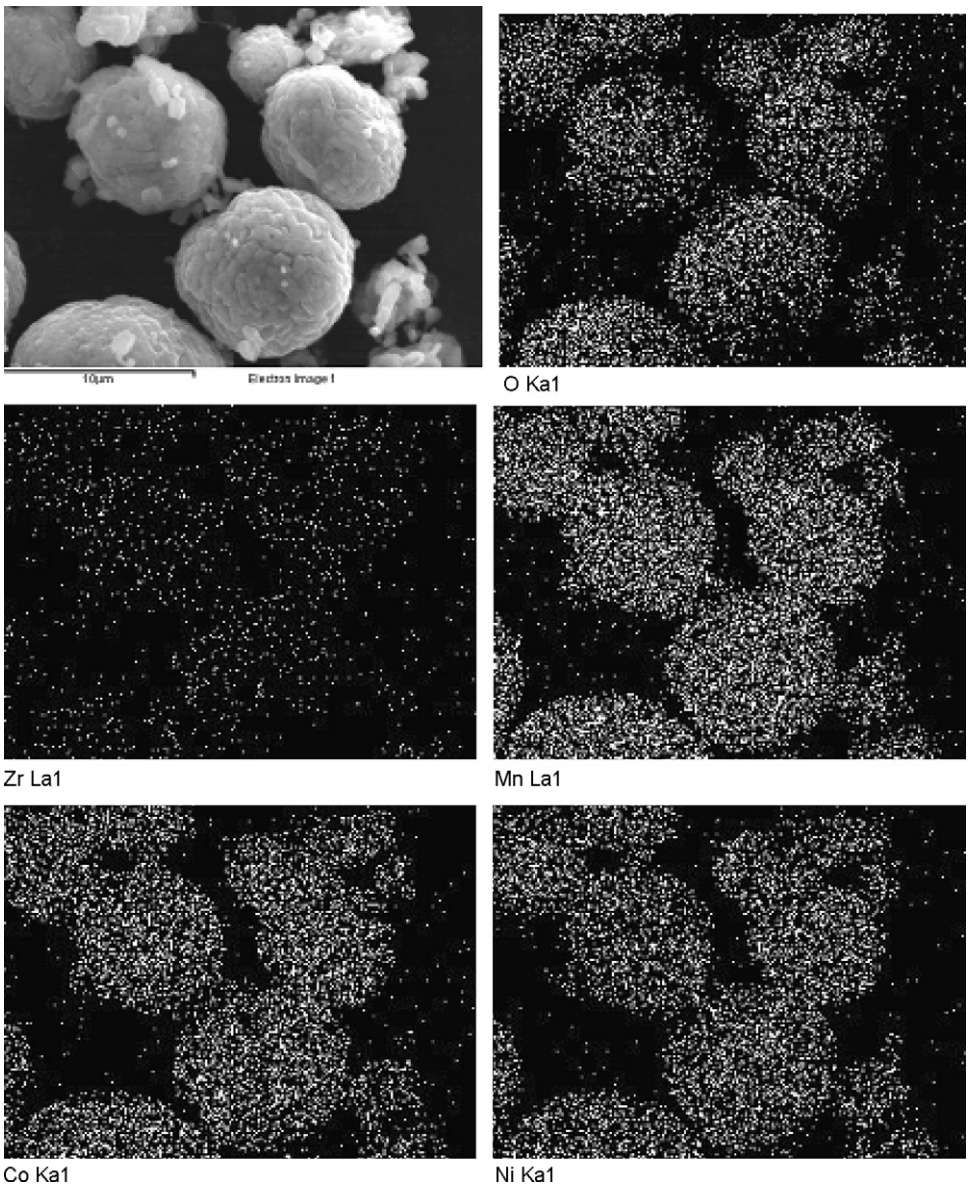

Fig. 2. EDS mapping patterns of 1% ZrO_2-modified $Li(Ni_{1/3}Co_{1/3}Mn_{1/3})O_2$.

structure with space group $R\bar{3}m$. Distinct splitting of the [(1 0 8), (1 1 0)] and [(0 0 6), (1 0 2)] peaks is observed in these patterns. Although the XRD patterns of bare, 0.5 and 1% ZrO_2-modified $Li(Ni_{1/3}Co_{1/3}Mn_{1/3})O_2$ samples show no significant difference, some impurity diffraction peaks are detected in the diffraction patterns of 2 and 3% ZrO_2-modified $Li(Ni_{1/3}Co_{1/3}Mn_{1/3})O_2$ in the 2θ range of 19–35°. As shown in the inset graph of Fig. 3, these impurity diffraction peaks can be identified as Li_2ZrO_3 (JSPDC card No. 75-2157). This result suggests that some Zr exists as Li_2ZrO_3 on the surface of $Li(Ni_{1/3}Co_{1/3}Mn_{1/3})O_2$. The lattice parameters were calculated using PowderX software. As shown in Fig. 4, lattice parameters of all samples vary obviously with Zr content. Lattice parameters a and c first increase with increasing Zr content and then decrease, but the trend of c/a value is the inverse. Usually, lattice parameter change means that a foreign element has become incorporated into the crystal lattice [14]. Therefore, we believe that some Zr^{4+} has diffused into the parent oxide after the high temperature treatment. Because the ion radius of Zr^{4+} (0.079 nm) [25] is larger than that of Co^{3+} (0.0545 nm), Ni^{2+} (0.069 nm) and Mn^{4+} (0.053 nm) [26], lattice parameters a and c increase as Zr/(Ni + Co + Mn) increases to 1%. The expansion in the lattice caused by a small amount of Zr^{4+} doping can benefit the transportation of Li^+ and enhance the rate capability of $Li(Ni_{1/3}Co_{1/3}Mn_{1/3})O_2$ [25,27]. However, lattice parameters a and c decrease for Zr/(Ni + Co + Mn) ≥ 2%. This could be ascribed to the monoclinic Li_2ZrO_3 on the surfaces of the parent oxides. As Fig. 4

Table 1
Concentration of Ni, Co, Mn in $(Ni_{1/3}Co_{1/3}Mn_{1/3})(OH)_2$ and 1% ZrO_2-modified $LiNi_{1/3}Co_{1/3}Mn_{1/3}O_2$.

Sample	Ni (mass%)	Co (mass%)	Mn (mass%)	Ni:Co:Mn (mole)
$(Ni_{1/3}Co_{1/3}Mn_{1/3})(OH)_2$	21.06	21.35	19.83	1.000:1.010:1.006
1% ZrO_2-modified $LiNi_{1/3}Co_{1/3}Mn_{1/3}O_2$	20.80	21.14	19.63	1.000:1.012:1.008

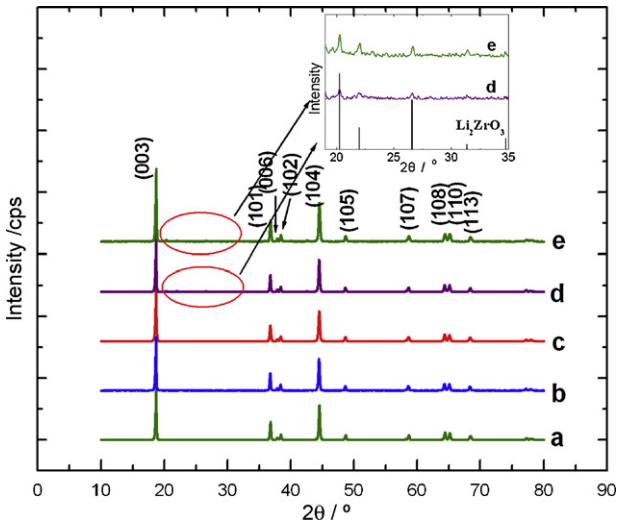

Fig. 3. XRD patterns of bare (a) and 0.5% (b), 1% (c), 2% (d), 3% (e) ZrO_2-modified $Li(Ni_{1/3}Co_{1/3}Mn_{1/3})O_2$. Inset graph is magnified XRD patterns of 2% (d) and 3% (e) ZrO_2-modified $Li(Ni_{1/3}Co_{1/3}Mn_{1/3})O_2$ in the 2θ range of 19–35°. The linear graph represents the standard diffraction peaks of Li_2ZrO_3 (JSPDC card No. 75-2157).

shows, the lattice parameter varies faster along the *a*-axis than the *c*-axis. The change in *c*/*a* with respect to Zr/(Ni + Co + Mn) is the reverse of the trend in lattice parameters *a* and *c*.

The intensity ratio of $I_{(003)}/I_{(104)}$ has been reported to be strongly correlated to undesirable cation mixing. The layered cathode materials with a high ratio of $I_{(003)}/I_{(104)}$ (>1.2) show a good electrochemical performance [28]. As shown in Fig. 4, all samples have a high ratio of $I_{(003)}/I_{(104)}$, and the ratio first increases then decreases with increasing Zr content. This trend is closely correlated to the electrochemical performance. Thus, 1% ZrO_2-modified $Li(Ni_{1/3}Co_{1/3}Mn_{1/3})O_2$ with the largest value of ratio I_{003}/I_{104} is expected to show the best electrochemical performance.

3.3. Analysis of the surface of ZrO_2-modified $Li(Ni_{1/3}Co_{1/3}Mn_{1/3})O_2$ by XPS

XPS was employed to examine the valence and the radial distribution of Zr and transition metal elements in the particles of ZrO_2-modified $Li(Ni_{1/3}Co_{1/3}Mn_{1/3})O_2$. Fig. 5a shows that the binding energies of electrons in Ni 2p3/2, Co 2p3/2 and Mn 2p3/2 are 854.7, 780.1 and 642.6 eV, respectively, in good agreement with the values in Ref. [21]. The result indicates that the dominant valences of Ni, Co and Mn are divalent, trivalent and tetravalent, respectively. Fig. 5b shows that the XPS spectrum of Zr 3d includes two peaks, Zr 3d5/2 (182.0 eV) and Zr 3d3/2 (184.3 eV). This result supports the fact that the valence of Zr is tetravalent [21]. Fig. 5c demonstrates the dependence of XPS spectra intensities on the etching time. With increasing etching time, the binding energy of electrons in Ni 2p3/2, Mn 2p3/2, Co 2p3/2, Zr 3d5/2 and O 1s remain constant, and the relative intensities of Ni 2p, Mn 2p and Co 2p first increase and then become stable. On the other hand, the relative intensity of O 1s first decreases and then become stable with increasing etching time. As shown in Fig. 5c, the relative intensity of the Zr 3d decreases gradually and the peak of Zr 3d3/2 becomes weaker until it disappears with increased etching time. The variation of the peak of Zr 3d3/2 indicates that the electron configuration of Zr is different on the surface and within the bulk of the material. The distributions of transition metal elements depends on the etching depth, as shown in Fig. 5d. The atomic concentration was calculated as M/(Ni + Co + Mn + Zr) (M can be set as Ni, Co, Mn, Zr). As shown in

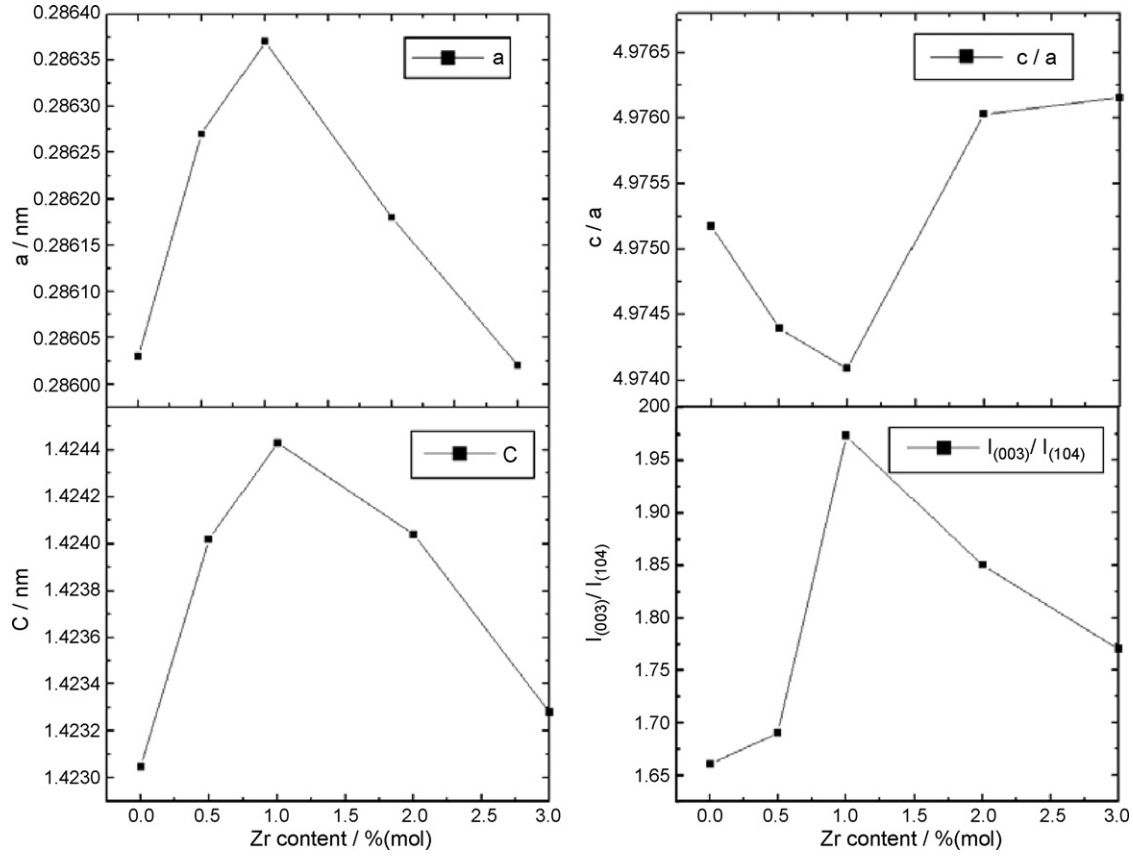

Fig. 4. Lattice parameters change with Zr amount and $I_{(003)}/I_{(104)}$ value for different ZrO_2-modified $Li(Ni_{1/3}Co_{1/3}Mn_{1/3})O_2$.

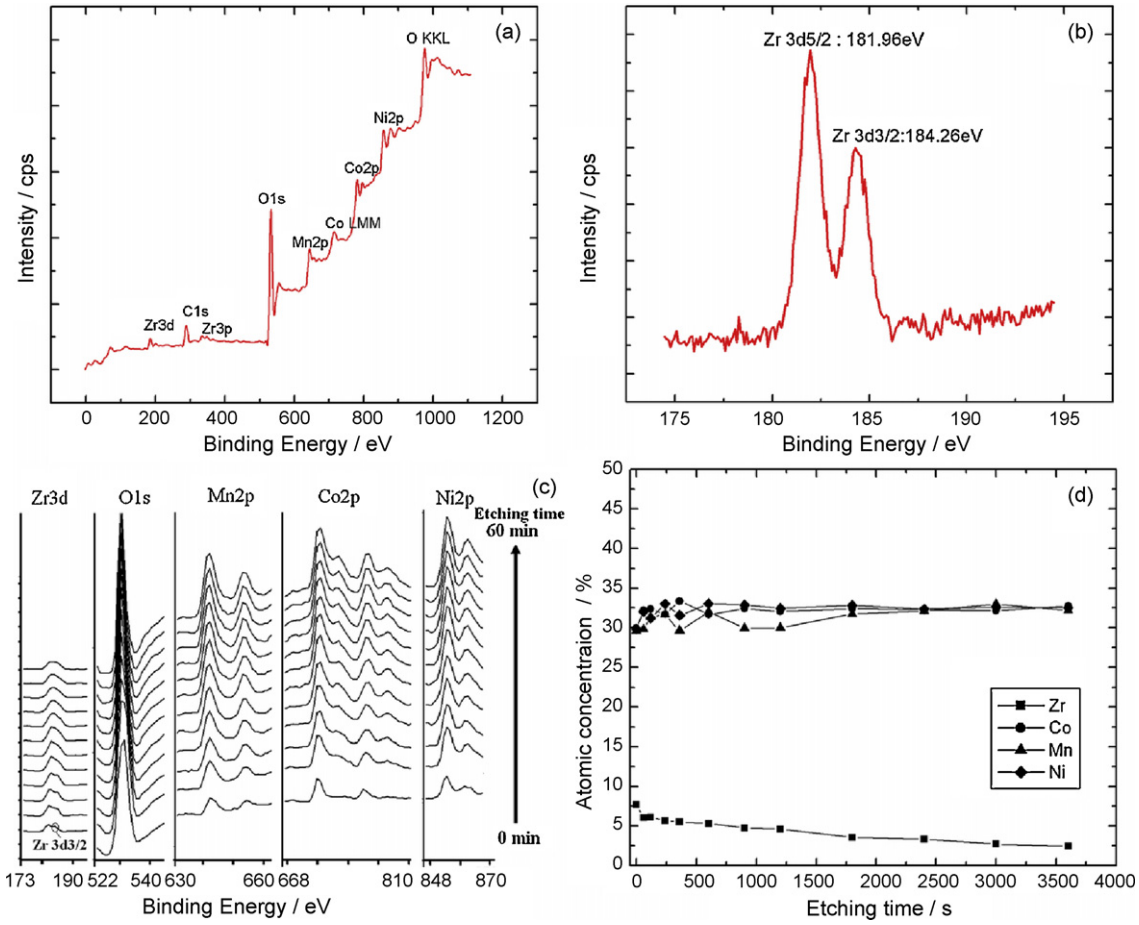

Fig. 5. (a) XPS spectra of 1% ZrO_2-modified $Li(Ni_{1/3}Co_{1/3}Mn_{1/3})O_2$. (b) Magnified XPS spectra of Zr 3d. (c) Dependence of XPS spectra of Ni 2p, Co 2p, Mn 2p, Zr 3d and O 1s on the etching time. (d) Depth element distribution profiles of 1% ZrO_2-modified $Li(Ni_{1/3}Co_{1/3}Mn_{1/3})O_2$. The atomic concentration was calculated by M/(Ni + Co + Mn + Zr) (M can be set as Ni, Co, Mn, Zr).

Fig. 5d, the ratio of Zr/(Ni + Co + Mn + Zr) is about 7.6% on the surface of the particle and gradually decreases with increasing etching time. When the Ar-ion etching was done for 60 min the ratio of Zr/(Ni + Co + Mn + Zr) decreased to about 2%. Meanwhile, the concentration of Ni, Co, and Mn first increase with increasing etching time and then become stable. These results and the XRD results support the fact that some Zr^{4+} enters the crystal lattice and that the Zr concentration decreases gradually from the surface to the bulk. The present result is a little different from the results reported by Myung et al., who reports that a coating metal oxide layer only exists on the surface of active materials [14].

3.4. Electrochemical properties of ZrO_2-modified $Li(Ni_{1/3}Co_{1/3}Mn_{1/3})O_2$

In order to study the electrochemical performance of the ZrO_2-modified $Li(Ni_{1/3}Co_{1/3}Mn_{1/3})O_2$ modified with different amounts of ZrO_2, coin cells were operated at 0.2*C* charging–discharging at room temperature. Fig. 6 shows the initial charge–discharge profile of these cells in the voltage ranges of 4.3–3.0 V (Fig. 6A) and 4.5–3.0 V (Fig. 6B). These results show that the charging and discharging curves of all cells are quite smooth, and the discharging average voltage does not change noticeably after ZrO_2 modification. Table 2 shows the charge and discharge capacities and initial irreversible capacities of all samples in the first cycle. When the ratio Zr/(Ni + Co + Mn) is 0.5 and 1%, the discharge capacity shows no significant decrease with ZrO_2 modification. However, when Zr/(Ni + Co + Mn) ≥ 2%, the discharge capacity decreases as the ratio increases. A small amount of Zr exists on the surface of particles as Li_2ZrO_3, which is conductive for Li^+, so it does not lead to large polarization and reversible capacity loss. However, Li_2ZrO_3 is an electrochemically inactive material, so too much Li_2ZrO_3 on the surface of a material will lead to capacity loss due to a decrease in active material [29]. The charge and discharge capacities of all

Table 2
Charge capacity, discharge capacity and irreversible capacity of all samples in the first cycle (capacity unit: mAh g^{-1}).

Sample	4.3–3.0 V			4.5–3.0 V		
	Charge capacity	Discharge capacity	Irreversible capacity	Charge capacity	Discharge capacity	Irreversible capacity
Bare	177.8	149.2	28.6	210.0	173.5	36.5
0.5% ZrO_2 modification	171.8	145.8	26.0	208.8	172.4	36.3
1% ZrO_2 modification	177.4	147.8	29.6	209.5	173.0	36.5
2% ZrO_2 modification	170.2	140.5	29.7	203.7	168.0	35.7
3% ZrO_2 modification	166.3	138.8	27.5	199.5	164.5	35.0

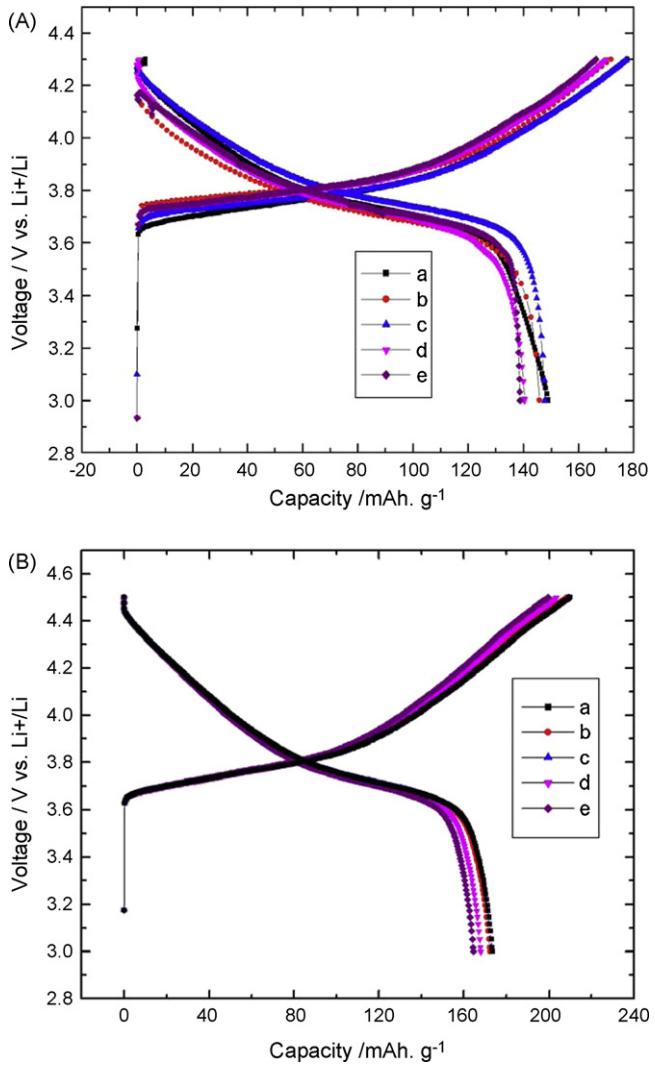

Fig. 6. The first charging and discharging curves of bare (a) and 0.5% (b), 1% (c), 2% (d) and 3% (e) ZrO_2-modified $Li(Ni_{1/3}Co_{1/3}Mn_{1/3})O_2$ in the voltage range of 4.3–3.0 V (A) and 4.5–3.0 V (B).

samples increase when the charge cut-off voltage increases from 4.3 to 4.5 V. The initial irreversible capacity shows the same trend. The increase of the initial irreversible capacity can be ascribed to the increase in electrolyte decomposition when the charge cut-off voltage is increased to 4.5 V [5,14].

Cycle performance was tested on the bare and 1% ZrO_2-modified $Li(Ni_{1/3}Co_{1/3}Mn_{1/3})O_2$ in the voltage ranges of 4.3–3.0 V and 4.5–3.0 V. As Fig. 7 shows, both bare and 1% ZrO_2-modified $Li(Ni_{1/3}Co_{1/3}Mn_{1/3})O_2$ exhibit good cycle performance at 4.3–3.0 V, but the bare $Li(Ni_{1/3}Co_{1/3}Mn_{1/3})O_2$ shows a significant capacity fading from 168.4 to 132.7 mAh g^{-1} during 100 cycles in the voltage range of 4.5–3.0 V. On the other hand, 1% ZrO_2-modified $Li(Ni_{1/3}Co_{1/3}Mn_{1/3})O_2$ shows a good capacity retention at 4.5–3.0 V. The discharge capacity is reduced from 166.1 to 164.6 mAh g^{-1} after 100 cycles, which only accounts for about 1% of the capacity loss. It is very clear that the cycle performance under high charge cut-off voltage is improved significantly by ZrO_2 modification. For the bare sample, the capacity loss can be ascribed to four factors: (1) lattice volume in the charge/discharge process; (2) cation mixing; (3) transition metal ion dissolution; (4) side reaction between electrode and electrolyte [5,7,14]. For the 1% ZrO_2-modified sample, the improvement in cycle performance might be ascribed to the special effect of Zr on $Li(Ni_{1/3}Co_{1/3}Mn_{1/3})O_2$. According to the XRD and XPS

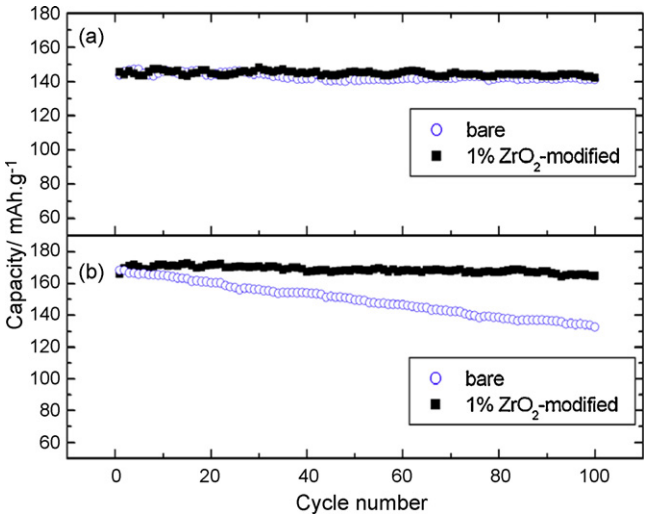

Fig. 7. Cycle performance comparison between bare material and 1% ZrO_2-modified $Li(Ni_{1/3}Co_{1/3}Mn_{1/3})O_2$ at 0.5*C* current charging and discharging in the voltage range of 4.3–3.0 V (a) and 4.5–3.0 V (b), respectively.

results, some Zr exists on the surface of particles as Li_2ZrO_3 and the rest diffuses into the crystal lattice of $Li(Ni_{1/3}Co_{1/3}Mn_{1/3})O_2$. The Li_2ZrO_3 on the surface of particles, acting as a protective layer, can decrease the direct contact between the electrolyte and electrode, and thus suppress the dissolution of transition metal elements and electrolyte decomposition. In addition, the strong Zr–O bond of Li_2ZrO_3 on the electrode surface is helpful for lowering the activity of oxygen on the electrode surface at high voltage. On the other hand, the Zr that diffuses into the crystal lattice may stabilize the structure during cycling [30].

The comparison of the rate capability between the bare and 1% ZrO_2-modified $Li(Ni_{1/3}Co_{1/3}Mn_{1/3})O_2$ is shown in Fig. 8. The cell was first charged to 4.3 V at 0.1*C* and then discharged to 3.0 V at currents of 0.2*C*, 0.5*C*, 1*C*, 2*C*, 3*C* and 5*C*. Fig. 8 shows that the capacity of the bare material decreases faster than that of the 1% ZrO_2-modified material when the discharging current is increased from 0.2*C* to 5*C*. The average discharging voltage also shows a similar phenomenon. The capacity of the bare material at 3*C* is 120.5 mAh g^{-1}, about 80% of that at 0.2*C*, while the 1% ZrO_2-modified material discharges at a capacity of 130.7 mAh g^{-1} at 3*C*, about 90% of that at 0.2*C*. Even at 5*C*, the capacity of the 1% ZrO_2-modified material still amounts

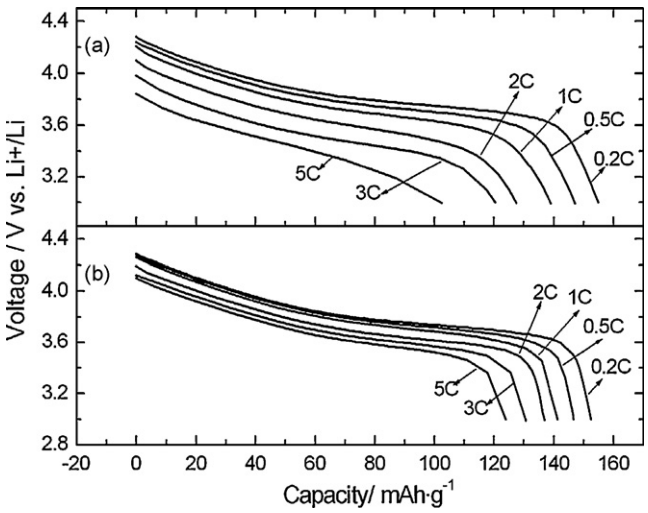

Fig. 8. Rate discharging capability of bare (a) and 1% ZrO_2-modified $Li(Ni_{1/3}Co_{1/3}Mn_{1/3})O_2$ (b).

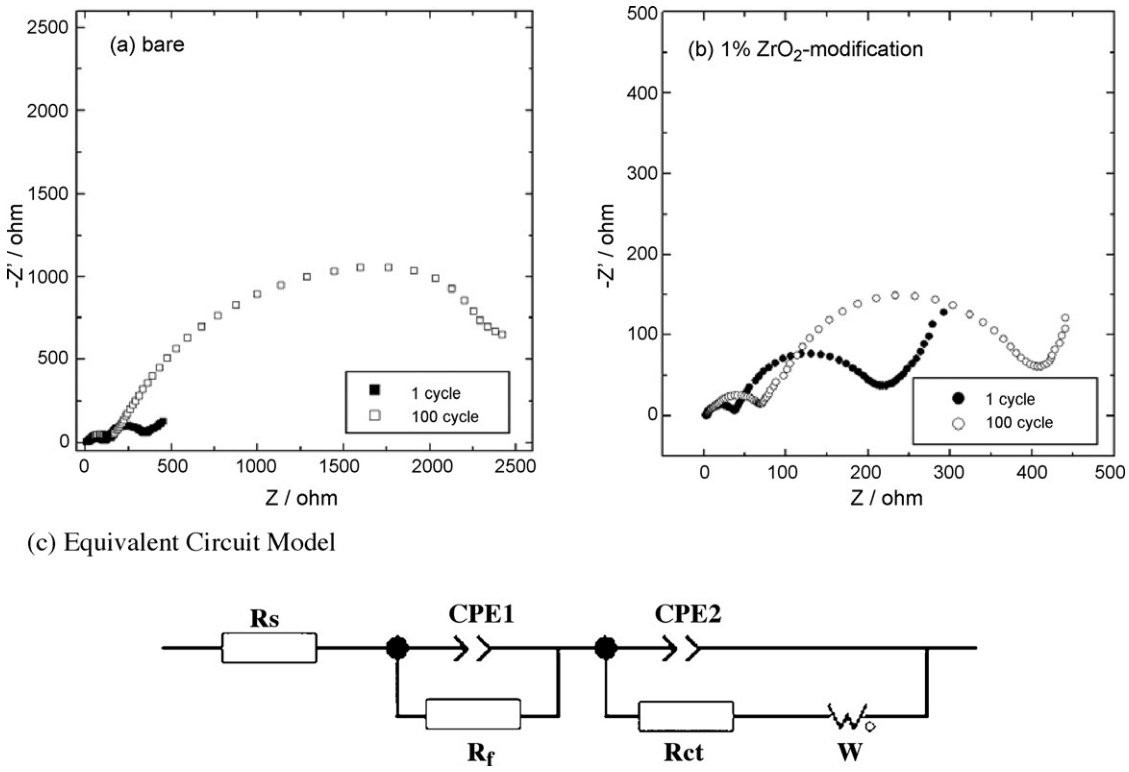

Fig. 9. EIS spectra of bare (a) and 1% ZrO_2-modified $Li(Ni_{1/3}Co_{1/3}Mn_{1/3})O_2$ (b). Corresponding equivalent circuit (c). R_s: solution resistance; R_f: surface film resistance; R_{ct}: charge transfer resistance; W: Warburg impedance.

to 124.0 mAh g^{-1}. These results show that the rate capability of $Li(Ni_{1/3}Co_{1/3}Mn_{1/3})O_2$ can be greatly enhanced by ZrO_2 modification. This can be ascribed to the increase in lattice parameters a and c caused by ZrO_2 modification [9,27,30].

In order to understand the improvement in the electrochemical properties by ZrO_2 modification, EIS experiments were performed. Fig. 9 shows the Nyquist plots measured using the coin cells of bare and 1% ZrO_2-modified $Li(Ni_{1/3}Co_{1/3}Mn_{1/3})O_2$ at a potential of 4.5 V after the 1st and 100th cycles. Generally, an impedance spectrum includes three parts: a semicircle in the high frequency range, a semicircle in the medium-to-low frequency range and a sloping line at low frequencies. The change of charge transfer resistance (R_{ct}) can be measured by calculating the diameter of the semicircles in the medium-to-low frequency range. As shown in Fig. 9, the R_{ct} of bare $Li(Ni_{1/3}Co_{1/3}Mn_{1/3})O_2$ increases to about 10 times the initial value after 100 cycles. However, the R_{ct} of 1% ZrO_2-modified $Li(Ni_{1/3}Co_{1/3}Mn_{1/3})O_2$ increases to only 2 times the initial value. This indicates that the increase in the charge transfer resistance during cycling is evidently suppressed via ZrO_2 modification. The dramatic increase in the charge transfer resistance of $Li(Ni_{1/3}Co_{1/3}Mn_{1/3})O_2$ can be caused by a side reaction between the electrolyte and the cathode [14]. The EIS results clearly indicate that the undesirable side reaction between the electrolyte and the cathode was significantly suppressed by ZrO_2 modification.

In order to clarify the effect of ZrO_2 modification on the Li^+ conductivity of $Li(Ni_{1/3}Co_{1/3}Mn_{1/3})O_2$ material, Li^+ diffusion coefficient (D_{Li}) was calculated by the following equation [31]:

$$D_{Li} = \frac{1}{2}\left[\left(\frac{V_m}{FAA_w}\right)\frac{dE}{dx}\right]^2 \quad (1)$$

In Eq. (1), V_m is the molar volume; F is the Faraday constant; A is the electrode area; A_w is the Warburg coefficient. In the Nyquist plot of EIS, the linear part impedance is directly related to Li^+ diffusion in material bulk. In the linear part of EIS, the imaginary resistance (Zimg) is the function of frequency (ω), and fit the following equation [32]:

$$Zimg = K - A_w\,\omega^{-1/2} \quad (2)$$

In Eq. (2), K is a constant. From the plot of Zimg as a function of $\omega^{-1/2}$ (not shown), the slope A_w can be obtained. The dE/dx can be obtained from the galvanostatic titration curve (not shown). According to Eqs. (1) and (2), D_{Li} of bare $Li(Ni_{1/3}Co_{1/3}Mn_{1/3})O_2$ charged to 4.5 V was valued to 5.56×10^{-9} $cm^2\ s^{-1}$, which is close to the result reported in Ref. [31]. D_{Li} of 1% ZrO_2-modified sample was valued to 1.12×10^{-8} $cm^2\ s^{-1}$. The increase of Li^+ diffusion coefficient increase can be ascribed to the Zr^{4+} incorporating into the bulk caused by ZrO_2 modification.

In order to investigate the effect of ZrO_2 modification on interfacial lithium ion transfer process of $Li(Ni_{1/3}Co_{1/3}Mn_{1/3})O_2$, temperature dependence of the interfacial lithium-ion transfer resistances (R_{ct}) was measured. The following equation [33] shows the connection of temperature, R_{ct} and activation energy:

$$\frac{T}{R_{ct}} = A\exp\left(-\frac{E_a}{RT}\right) \quad (3)$$

Here E_a is the activation energy; T is the absolute temperature; R is the gas constant; R_{ct} is the interfacial lithium-ion transfer resistance; A is the pre-exponential factor. The following equation can be deduced from Eq. (3):

$$\log\frac{T}{R_{ct}} = \log A - \frac{E_a}{2.303R}\frac{1}{T} \quad (4)$$

According to the above equation, the activation energy was obtained by calculating the slope of the plot of $lg(T/R_{ct})$ as a function of $1000/T$. As shown in Fig. 10, these data show good linearity. The activation energy of Li^+ transfer reaction of bare and 1% ZrO_2-modified $Li(Ni_{1/3}Co_{1/3}Mn_{1/3})O_2$ were valued to 70.61 and 63.55 kJ mol^{-1}, respectively. Smaller activation energy of ZrO_2-modified sample indicates that ZrO_2 modification can

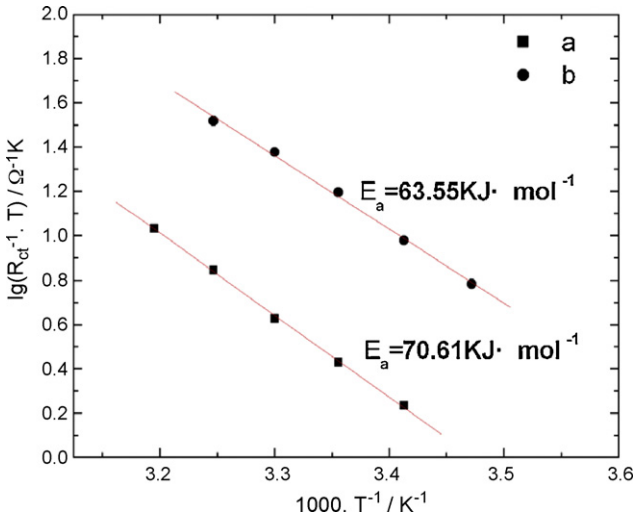

Fig. 10. Temperature dependency for interfacial lithium-ion transfer resistance of bare (a) and 1% ZrO_2-modified $Li(Ni_{1/3}Co_{1/3}Mn_{1/3})O_2$ (b) in 1.0 mol L^{-1} $LiPF_6$/(EC:EMC:DEC = 1:1:1).

speed up the interfacial lithium ion transfer reaction occurring on $Li(Ni_{1/3}Co_{1/3}Mn_{1/3})O_2$/electrolyte interface.

4. Conclusions

In this paper, we introduce a modified ZrO_2-coating process to improve the electrochemical performance of $Li(Ni_{1/3}Co_{1/3}Mn_{1/3})O_2$. Namely, the ZrO_2-coating was done on the intermediate $(Ni_{1/3}Co_{1/3}Mn_{1/3})(OH)_2$ instead of on $Li(Ni_{1/3}Co_{1/3}Mn_{1/3})O_2$. XRD and XPS results show that one part of Zr covers the surface of electrode material of $Li(Ni_{1/3}Co_{1/3}Mn_{1/3})O_2$ in the form of a Li_2ZrO_3 coating layer, and the rest diffuses into the crystal lattice of $Li(Ni_{1/3}Co_{1/3}Mn_{1/3})O_2$. The surface coating layer of Li_2ZrO_3 can improve the cycle performance by suppressing the side reactions between the electrode and the electrolyte, while the incorporation of Zr in layered crystal can modify the rate capability by increasing the lattice parameters. Compared to the bare material, 1% ZrO_2-modified $Li(Ni_{1/3}Co_{1/3}Mn_{1/3})O_2$ prepared by this process shows a better cyclability and rate capability. EIS results show that the increase in the charge transfer resistance during cycling was suppressed significantly by ZrO_2 modification. The result of electrode kinetics measurement obtained from EIS indicates that ZrO_2 modification is effectual to increase Li^+ diffusion coefficient and reduce the active energy of interfacial Li^+ transfer reaction of $Li(Ni_{1/3}Co_{1/3}Mn_{1/3})O_2$.

Acknowledgements

This work was supported by 973 Project of China (No. 2009CB220100). We gratefully acknowledge Mr. Jinglin Xie for his XPS measurements.

References

[1] T. Ohzuku, Y. Makimura, Chem. Lett. 7 (2001) 642–643.
[2] N. Yabuuchi, T. Ohzuku, J. Power Sources 119–121 (2003) 171–174.
[3] D.-C. Li, T. Muta, L.-Q. Zhang, M. Yoshio, H. Noguchi, J. Power Sources 132 (2004) 150–155.
[4] J. Kim, C. Park, Y. Sun, Solid State Ionics 164 (2003) 43–49.
[5] K.M. Shaju, G.V.S. Rao, B.V.R. Chowdari, Electrochim. Acta 48 (2002) 145–151.
[6] G.-H. Kim, M.-H. Kim, S.-T. Myung, Y.K. Sun, J. Power Sources 146 (2005) 602–605.
[7] G.-H. Kim, J.-H. Kim, S.-T. Myung, C.S. Yoon, Y.-K. Sun, J. Electrochem. Soc. 152 (2005) A1707–A1713.
[8] H.-S. Kim, M. Kong, K. Kim, I.-J. Kim, H.-B. Gu, J. Power Sources 171 (2007) 917–921.
[9] S.-H. Na, H.-S. Kim, S.-I. Moon, Solid State Ionics 176 (2005) 313–317.
[10] J. Choi, A. Manthiram, J. Electrochem. Soc. 152 (2005) A1714–A1718.
[11] Y.-K. Sun, Y.-S. Lee, M. Yoshio, K. Amine, Electrochem. Solid-State Lett. 5 (2002) A99–A102.
[12] Y. Iriyama, H. Kurita, I. Yamada, T. Abe, Z. Ogumi, J. Power Sources 137 (2004) 111–116.
[13] J. Cho, Y.J. Kim, B. Park, Chem. Mater. 12 (2000) 3788–3791.
[14] S.-T. Myung, K. Izumi, S. Komaba, Y.-K. Sun, H. Yashiro, N. Kumagai, Chem. Mater. 17 (2005) 3695–3704.
[15] J. Cho, T.-J. Kim, Y.J. Kim, B. Park, Electrochem. Solid-State Lett. 4 (2001) A159–A161.
[16] J. Cho, Y.J. Kim, T.J. Kim, B. Park, Angew. Chem. Int. Ed. Engl. 40 (2001) 3367–3369.
[17] Y.-M. Lin, H.-C. Wu, Y.-C. Yen, Z.-Z. Guo, M.-H. Yang, H.-M. Chen, H.-S. Sheu, N.-L. Wu, J. Electrochem. Soc. 152 (2005) A1526–A1532.
[18] S.M. Lee, S.H. Oh, J.P. Ahn, W.I. Cho, H. Jang, J. Power Sources 159 (2006) 1334–1339.
[19] Z.R. Zhang, H.S. Liu, Z.L. Gong, Y. Yang, J. Power Sources 129 (2004) 101–106.
[20] G.T.-K. Fey, C.-Z. Lu, J.-D. Huang, T.P. Kumar, Y.-C. Chang, J. Power Sources 146 (2005) 65–70.
[21] D. Li, Y. Kato, K. Kobayakawa, H. Noguchi, Y. Sato, J. Power Sources 160 (2006) 1342–1348.
[22] Y. Kim, H.S. Kim, S.W. Martin, Electrochim. Acta 52 (2006) 1316–1322.
[23] H. Cao, B. Xia, Y. Zhang, N. Xu, Solid State Ionics 176 (2005) 911–914.
[24] H.-S. Kim, Y. Kim, S.-I. Kim, S.W. Martin, J. Power Sources 161 (2006) 623–627.
[25] H.-S. Kim, T.-K. Ko, B.-K. Na, W.I. Cho, B.W. Chao, J. Power Sources 138 (2004) 232–239.
[26] D.D. MacNeil, Z.H. Lu, J.R. Dahn, J. Electrochem. Soc. 149 (2002) A1332–A1336.
[27] S. Venkatraman, J. Choi, A. Manthiram, Electrochem. Commun. 6 (2004) 832–837.
[28] T. Ohzuku, A. Ueda, M. Nagayama, J. Electrochem. Soc. 140 (1993) 1862–1870.
[29] M.M. Thackeray, C.S. Johnson, J.-S. Kim, K.C. Lauzze, J.T. Vaughey, N. Dietz, D. Abraham, S.A. Hackney, W. Zeltner, M.A. Anderson, Electrochem. Commun. 5 (2003) 752–758.
[30] B. Lin, Z. Wen, Z. Gu, X. Xu, J. Power Sources 174 (2007) 544–547.
[31] K.M. Shaju, G.V.S. Rao, B.V.R. Chowdari, J. Electrochem. Soc. 151 (2004) A1324–A1332.
[32] J. Ni, H. Zhou, J. Chen, X. Zhang, Electrochim. Acta 53 (2008) 3075–3083.
[33] N. Nakayama, T. Nozawa, Y. Iriyama, T. Abe, Z. Ogumi, K. Kikuchi, J. Power Sources 174 (2007) 695–700.